Supporting Information

Here, we present details of various aspects of the wrinkling process in support of observations made in the main report. These supplementary results focus on secondary observations of the morphological behavior of wrinkled surfaces under conditions similar to those outlined in the main text. However, in some cases the general morphologies do not match up exactly with those reported in Figure 1, due to inconsistencies in the UVO treatment process associated with either a) the age of the UV bulb (extent of oxidation decreases over the lifetime of the bulb) or b) the configuration of the sample in the oxidation chamber. The latter point is most relevant to the prestrained (i.e. clamped) samples, as the presence of the clamp alters the airflow above the surface of the sample, resulting in changed oxidation compared to unclamped samples.

Figure S1 depicts two samples as seen via normal optical microscopy (OM) and differential interference contrast (DIC) microscopy. The samples were treated with UVO for 10 and 15 minutes respectively, and swollen in 100% ethanol. Under OM, both samples appear flat, but under DIC, small-amplitude prebuckling undulations are highlighted in the 15-minute sample which are not observed in the 10-minute sample. The lengthscale of prebuckling can be determined via Fourier analysis (insets), and is similar to the wrinkle wavelength for a given UVO treatment time.

Figure S2 shows examples of samples displaying multiple buckling modes on single surfaces. These observations were prevalent for samples with a high UVO treatment time (45 or 60 minutes) and a moderate ethanol vapor fraction (40-70% in reservoir). The reason for this behavior is unclear, but may suggest slight differences in the extent of oxidation at different areas of the surface. Most significantly, these multiple modes occur at low values of overstress.

The transition of the wrinkle orientation across the surface of the prestrained samples is depicted in Figure S3. The stitched images were captured at the midpoint of the wrinkling beam surface. Figure S2a shows a smooth transition from y-aligned ridges to x-aligned ridges via a gradual shift of the ridge orientation. The x-aligned ridges then gradually acquire more and more herringbone characteristic as the distance from the clamped area increases, until at the far right end of the beam, all orientation is lost and the wrinkles are in a labyrinthine pattern. Figure S3b also shows similar y- and x-orientation, but the transitional area between these two regions is actually unwrinkled. According to our FEM data in Figure 3a, a region exists shortly beyond the clamp in which both σ_{xx} and σ_{yy} are compressive, leading to a tensile prestress. We believe that under these conditions, the prestress is sufficient to lower the subsequently generated swelling stress below σ_c while the remainder of the sample is at or above σ_c. At the far right end of the sample, coalesced dimples are observed with no preferred orientation.

Figure S4 depicts pure dimple phases at slightly varying treatment conditions, indicating the accessibility of the dimple phase via a small but finite range of conditions. There is a noticeable variation of the characteristic pattern length between the two samples, suggesting a true difference in the extent of oxidation.

Figure S5 expands the morphological characterizations of Figure 5 to include UVO treatment and ethanol vapor fraction data. A clear trend is seen for all UVO times of increasing overstress with ethanol vapor fraction, and the tendency of higher UVO times to reach higher overstress is generally conserved.

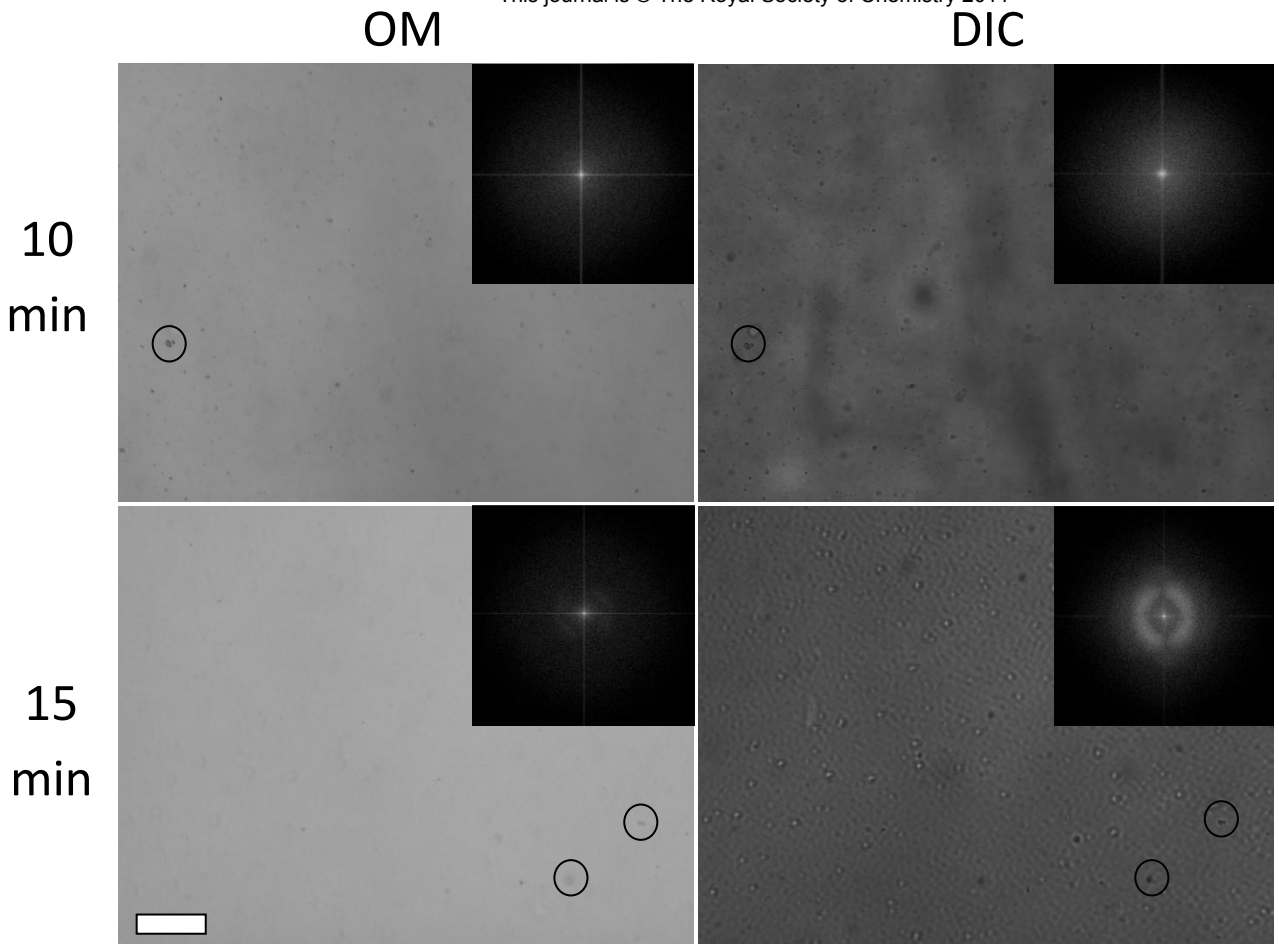

Figure S1: Samples viewed under normal optical microscopy (OM) and differential interference contrast microscopy (DIC) at the same location, exposed to vapor from a reservoir of 100% ethanol. Both samples appear flat under OM, but DIC mode reveals prebuckling in the 15-minute UVO sample, while no prebuckling is observed for the 10-minute UVO sample. Black circles indicate surface defects present in both images. Insets: Fast Fourier transforms of the images, revealing a characteristic length scale in the prebuckled sample, approximating the wrinkle wavelength. Scale bar is 250 µm.

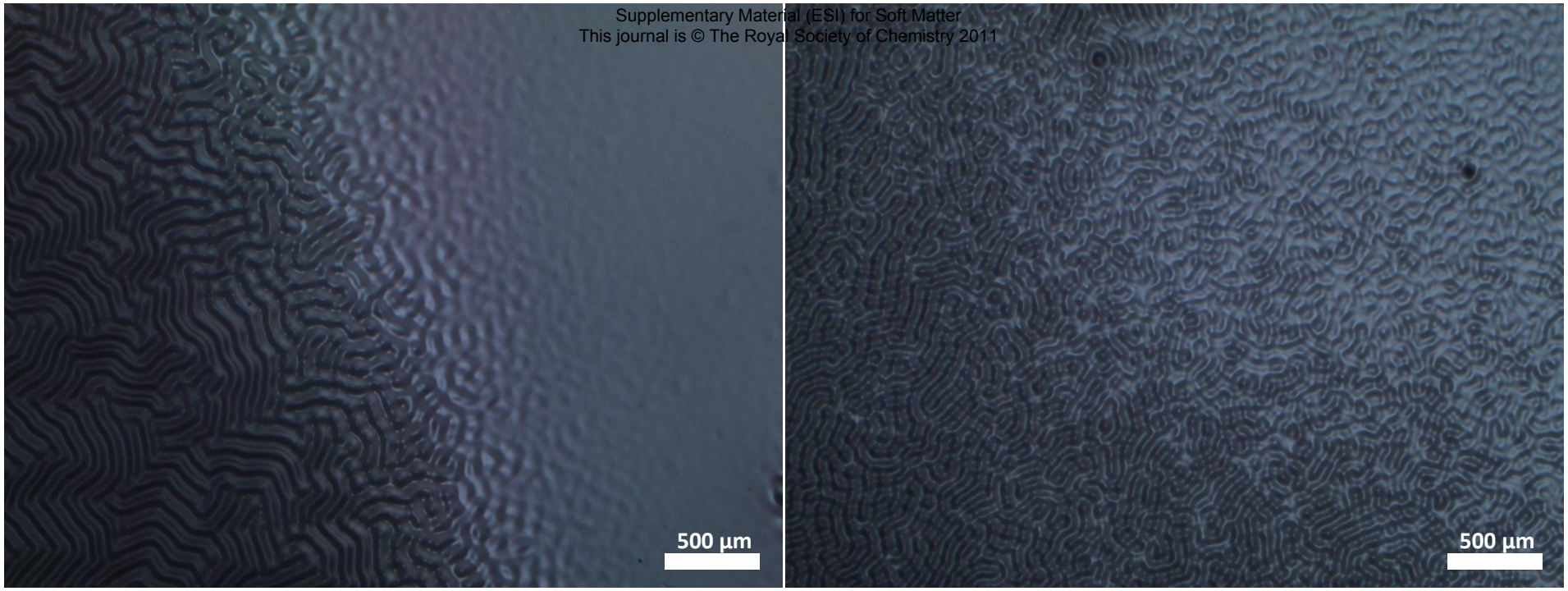

Figure S2: Examples of co-existing morphologies on the surface of swollen wrinkled surfaces at equilibrium. **a)** Abrupt lateral transition from labyrinthine ridges to flat (unbuckled) regions; UVO treatment time = 60 min., reservoir ethanol fraction = 60%. **b)** Gradual transition from ridge-like patterns of coalesced dimples towards flat regions (not in frame). UVO treatment time = 45 min., reservoir ethanol fraction = 70%.

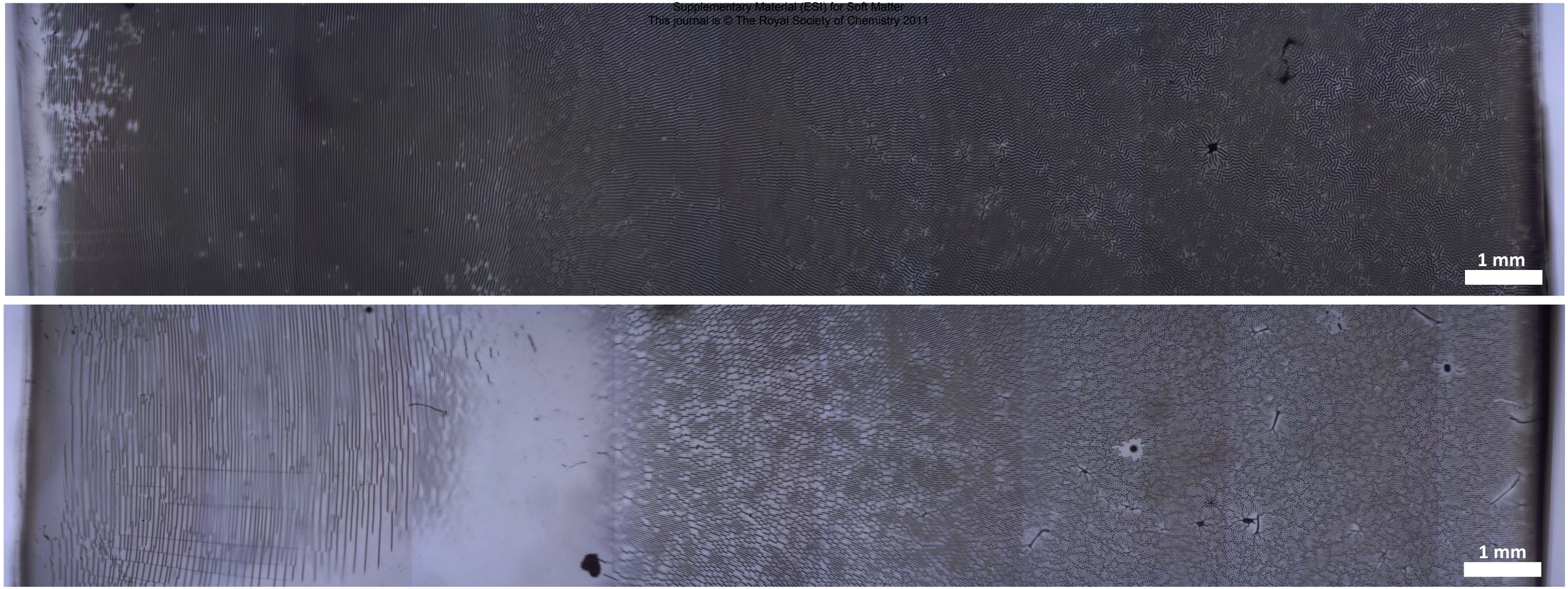

Figure S3: Stitched images depicting the morphological transitions of wrinkled beams across varying states of prestrain. Prestrain is induced by clamping the left ends of the beams during oxidation. **a)** Beam treated with UVO for 30 minutes, exhibiting the labyrinth morphology on the unclamped end. **b)** Beam treated with UVO for 20 minutes, resulting in a coalesced dimple morphology on the unclamped end. Dark spots represent dust particles adhered to the PDMS. The observed morphology on the unclamped end of b) is noted to differ from the pure dimples observed in Figure 1; this is likely due to differences in UVO process between the two experiments, including effects resulting from the presence of the clamp as well as differences in the age of the UV bulb.

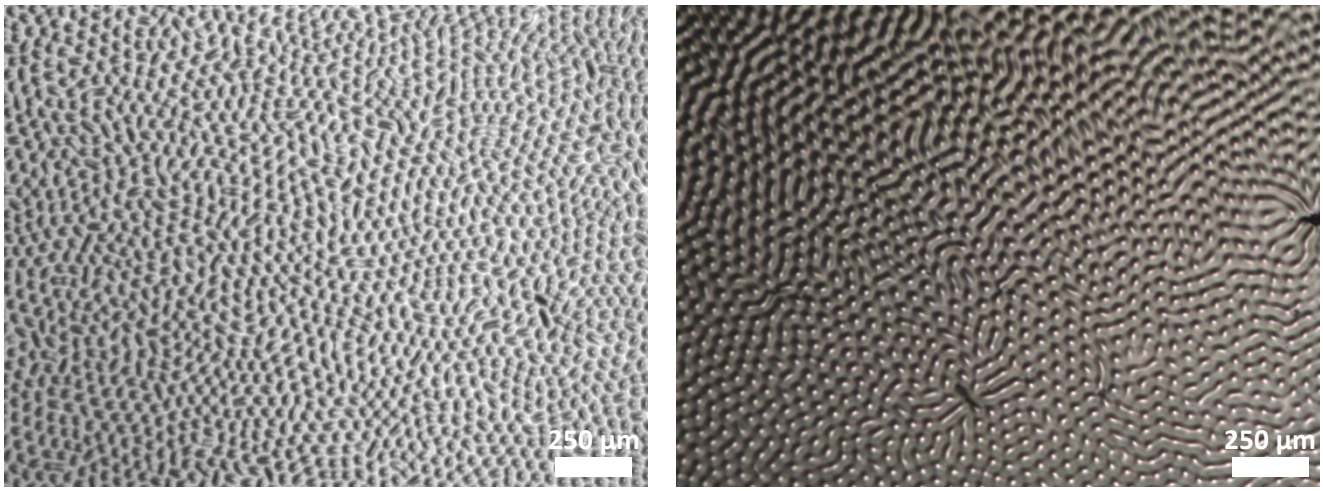

Figure S4 Stable dimple arrays formed at different conditions: **a)** UVO time: 18 minutes, ethanol reservoir fraction: 100%; **b)** UVO time 20 minutes, ethanol reservoir fraction 90%. Note the slightly larger feature size of b). As in Figure S2, morphologies differ slightly from those reported in Figure 1 due to differences in the age of the UV lamp between the different samples.

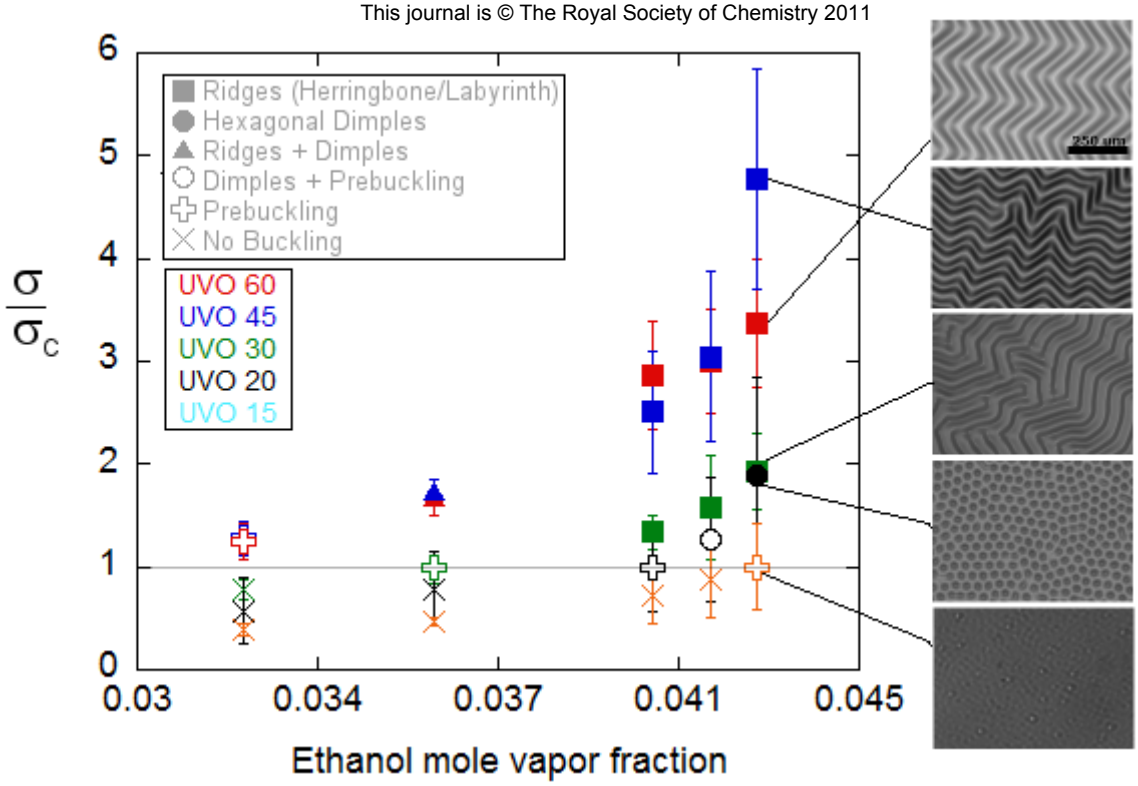

Figure S5: Plot of overstress as a function of ethanol vapor fraction for various UVO treatment times. Data point shapes indicate dominant morphology as depicted in Figure 1.